



# Three-dimensional Effects of Hydraulic Conductivity Enhancement and Desaturation around Mined Panels

J. LIU†

D. ELSWORTH‡

*Changes in the three-dimensional hydraulic conductivity field that accompany undermining by a longwall panel are evaluated to define the potential for changes in flow patterns and desaturation. Relations linking changes in conductivity with the mining-induced strain field that develops around the advancing face are defined through the assumption of an equivalent porous medium with the strain partition between fractures and matrix apportioned relative to respective deformation constants. Model results are validated against behavior recorded at a well instrumented field site, replicating the complex steady flow pattern that develops around an advancing longwall face. Significant hydraulic conductivity increases are restricted to strata at shallow depth, ahead of the advancing face, and to deep zones behind the face, particularly in the caving zone and abutment shear zones. These very large increases in conductivity at depth, that include the out-of-section conductivity enhancement that develops along the panel rib, exercise primary control on induced water level changes and the potential for saturation. Zones of desaturation are readily defined, with these enabling locations of well vulnerability (to water loss) to be identified. These zones of vulnerability are directly above the panel, with their extent potentially modulated by the presence and the location of flatlying layers of low conductivity. The complex response recorded in the near-face region mandates use of three-dimensional models to adequately represent observed behavior. © 1998 Published by Elsevier Science Ltd*

## 1. INTRODUCTION

Underground mining by *full extraction* methods, such as longwall mining, is becoming increasingly popular for mining uninterrupted and near horizontal seams. Longwall mining involves extracting coal in large blocks called panels using a mechanized shearer. The full thickness, of perhaps 1–2 m, is removed and panel extents are typically 200–350 m wide and up to 3000 m in length. Multiple panels comprise a single mining operation. With this method, the mine roof is supported with hydraulic supports that automatically advance as mining progresses. As the supports move, the mine roof is allowed to collapse into the mine void. Strata above the mine level are altered as the mine roof caves behind the shields (hydraulic supports), creating zones where blocks of rock fill the mine void, or fracture or deform

as rock layers warp downward. These alterations in overburden characteristics potentially induce large strains in the overlying strata that in turn may result in a strongly heterogeneous and anisotropic hydraulic conductivity field. This strain-dependent conductivity field is of special importance in evaluating the potential impact of longwall mining on ground water resources. A number of studies have indicated that subsidence-induced fracturing may increase hydraulic conductivity magnitudes by up to several orders of magnitude [1–4]. Consequently, the local ground water system may be appreciably altered [5–8]. Despite the acknowledgement that changes in conductivity may be substantial, few studies document the interaction between deformation of the overlying strata and its influence on ground water flow [9–13]. These studies have reported the research results for two-dimensional geometries but neglected the true three-dimensional complexity of the zone immediately surrounding the advancing face. This study represents the first known study documenting the complex three-dimensional response anticipated around

†Department of Mining, Minerals and Materials Engineering, The University of Queensland, Brisbane, QLD 4072, Australia.

‡Department of Mineral Engineering, Pennsylvania State University, University Park, PA 16802, U.S.A.

the advancing mining face through implementing the prescribed displacement boundary conditions, instead of the prescribed force boundary conditions [9–13], around a longwall panel. The following document is an approach to define the form of this interaction, in a predictive capacity, enabling the influence on the ground water system to be defined.

The undermined strata typically have a complicated internal structure and stress state, both of which are, in large part, *unknown* and perhaps *unknowable*. This would appear to make solution for the revised, mining-induced, conductivity field intractable. However, some alternatives may be pursued to avoid using parameters that are unlikely available in practice. The subsidence field that develops around a longwall panel is relatively insensitive to the material properties of deformation modulus and strength due to the displacement (subsidence) controlled nature [14,15]. Therefore, the mining-induced strain field, defined by the subsidence profile, may also be decoupled from the material parameters describing the overlying strata. Once the strain field is defined as unique for any given mining geometry, changes in the ground water budget may be evaluated providing a link may be established between induced strains and changes in hydraulic conductivity. This is the underlying scientific rationale of this research.

## 2. EVALUATION OF MINING-INDUCED STRAIN FIELD

The complex 3-D strain field that develops around the advancing face of a longwall panel may be evaluated only with recourse to numerical methods. This local behavior is significant, since the distribution of strains, and hence conductivities, are strongly conditioned by hysteretic and path dependent behavior in the 3-D strain regime that develops around the advancing face, even though the ultimate panel section is amenable to plane strain representation. However, even as a plane section with regard to displacement behavior, the flow behavior remains implicitly three-dimensional, with important out-of-section flow components.

In this work, a 3-D finite element model is developed that incorporates strain softening following failure, assuming that changes in the groundwater regime are trivial in comparison with the massive changes in total stress that accompany mining. Previous evaluation of 2-D fully coupled (poroelastic) systems involving single [9] and dual [10] porosity behavior have confirmed the short-lived nature of the transient poroelastic effects. Similarly, 2-D analyses with steady-state coupling for effective stresses [11] have indicated the trivial contribution of effective stresses over the massive realignment of total stresses conditioned by mining. Correspondingly, coupling in the following is restricted to consideration of changes in hydraulic conductivity, coupled to the evolving strain regime. This simplification is especially important for 3-D analyses, enabling a significant reduction in execution time, with no significant loss of relevance in tracking processes.

### 2.1. Finite element representation

It is assumed that the rock mass is isotropic but heterogeneous. The resulting finite element formulation for the solid phase is symbolically defined as

$$\mathbf{K}_s \mathbf{d} = \mathbf{f} \quad (1)$$

where  $\mathbf{K}_s$  is the stiffness matrix of the solid phase,  $\mathbf{d}$  is the nodal displacement vector, and  $\mathbf{f}$  is the nodal force vector. The stiffness matrix,  $\mathbf{K}_s$ , in equation (1) is defined as

$$\mathbf{K}_s = \iiint_v \mathbf{B}^T \mathbf{D} \mathbf{B} \, dx \, dy \, dz \quad (2)$$

where  $\mathbf{B}$  is a geometric matrix,  $\mathbf{D}$  is material properties matrix and a function of the elastic modulus,  $E$ , and the Poisson ratio,  $\nu$ , and  $v$  is the volume. The mining-induced strain vector can be obtained as

$$\Delta \epsilon = \mathbf{B} \mathbf{d}. \quad (3)$$

The displacement controlled nature of subsidence is implemented in the finite element model (FEM) through two different non-linear material models representing the overburden failure and the coal extraction, respectively. These two non-linear material models are presented in the following.

### 2.2. Representation of overburden failure

Notice that the  $\mathbf{B}$  matrix in equation (2) remains fixed during the solution procedure, and only the  $\mathbf{D}$  matrix has to be adapted at each iteration. This is achieved at the end of each iteration by calculating the maximum principal stress,  $\sigma_{11}$ , and modifying the “effective” elastic parameters as

$$E = \begin{cases} E_0 & \sigma_{11} < 0 \\ \frac{E_0}{R_c} & \sigma_{11} \geq 0 \end{cases} \quad (4)$$

$$\nu = \begin{cases} \nu_1 & \sigma_{11} < 0 \\ \nu_2 & \sigma_{11} \geq 0 \end{cases} \quad (5)$$

where  $E$  is elastic modulus of the overburden,  $E_0$  is elastic modulus of elements in compression,  $E_0/R_c$  is elastic modulus of elements in extension,  $\nu_1$  is Poisson ratio of elements in compression,  $\nu_2$  is Poisson ratio of elements in extension, and  $\sigma_{11}$  is the maximum principal stress. The magnitude of  $R_c$  is obtained by matching the “field-measured” or estimated maximum subsidence.

### 2.3. Representation of coal extraction

A similar non-linear modulus model is used to represent the process of coal extraction. The main advantage of this method is that elements do not have to be removed from the mesh in order to simulate coal extraction, and excavation boundary tractions do not need to be calculated. More importantly, the prescribed displacement boundary conditions around the longwall panel can be successfully implemented. The  $\mathbf{D}$  matrix, as shown in equation (2), for in-panel elements has to be

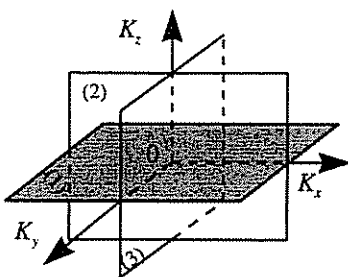


Fig. 1. Conceptual model for the effect of fractures on the principal hydraulic conductivities. The bracketed numbers represent three sets of orthogonal fracture planes.

adapted at each iteration. This is achieved at the end of each iteration by calculating the vertical strain  $\epsilon_z$

$$E_p = \begin{cases} E_{p0} & \epsilon_z > -1,0 \\ 10^n E_{p0} & \epsilon_z \leq -1,0 \end{cases} \quad (6)$$

where  $E_p$  is modulus of the material comprising the panel,  $E_{p0}$  is initial modulus of the panel material (before mining) and  $\epsilon_z$  is vertical strain within the panel material. This simple model prevents the interpenetration of the panel roof and floor by changing the panel modulus at contact, where  $n$  may be assigned any reasonable large numbers.

### 3. EVALUATION OF POST-MINING CONDUCTIVITY FIELD

The dependence of post-mining hydraulic conductivity on mining-induced strain (or stress) is frequently noted [1,2,16], but no three-dimensional quantitative relations between them are available. These relations are developed based on the reported two-dimensional results [9,10,13] and applied to the determination of the post-mining strain-dependent hydraulic conductivity field in the following.

#### 3.1. Three-dimensional relations

Two-dimensional relations [13] linking changes in hydraulic conductivity to changes in applied strain may be extended for flow in the third dimension. For three-dimensional orthogonally fractured media, changes in one-directional hydraulic conductivity are a function of mining-induced strains in the other two orthogonal directions, as illustrated in Fig. 1. Assuming that the rock matrix is functionally impermeable, and that the dominant fluid flow within the fractures may be defined by an *equivalent parallel plate model*, enables changes in hydraulic conductivity to be determined if induced strains may be adequately partitioned between fracture and solid matrix. Fracture and matrix deformation are both linear, and deformations in normal closure or extension are the predominant conductivity enhancing mode. Deformations are fully recoverable in this mode, with strains defined positive in extension. Conductivity changes in compression are typically truncated by a lower threshold defining the limits of conductivity reduction. Strains are partitioned between fracture and matrix as defined by the modulus reduction factor. Additionally, fracture spacing,  $s$ , does not change post-mining. Under these assumptions the changes in hydraulic conductivity in the three orthogonal directions,  $K_x$ ,  $K_y$  and  $K_z$ , are conditioned by fracture apertures,  $b_x$ ,  $b_y$ ,  $b_z$ , and fracture spacings,  $s_x$ ,  $s_y$ , and  $s_z$ , defined with the fracture plane normal aligned in the coordinate direction.  $\Delta\epsilon_x$ ,  $\Delta\epsilon_y$  and  $\Delta\epsilon_z$  are mining-induced strains in the  $x$ -,  $y$ - and  $z$ -directions, respectively, and  $R_m$  is a modulus reduction ratio (ratio of rock mass modulus to rock matrix modulus) that apportions changes in strain between the fracture and matrix material. From this, conductivity magnitudes may be defined relative to the pre-mining conductivity field,  $K_{x0}$ ,  $K_{y0}$ ,  $K_{z0}$ , as

$$K_x = \frac{1}{2} K_{x0} [(1 + \beta_x \Delta\epsilon_x)^2 + (1 + \beta_x \Delta\epsilon_z)^2] \quad (7)$$

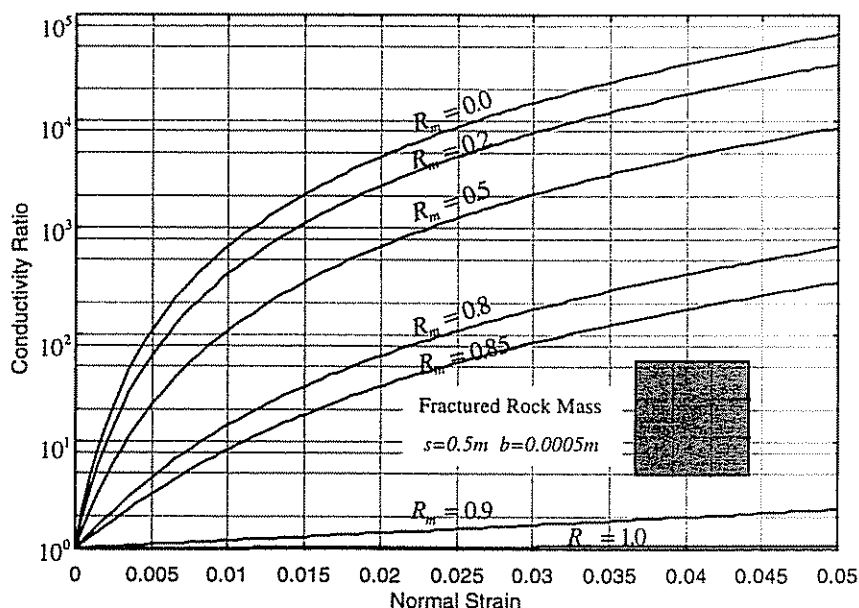


Fig. 2. Relationship between modulus reduction ratio,  $R_m$ , and normal strain,  $\Delta\epsilon$ , under conditions of fracture spacing  $s = 0.5$  m and aperture  $b = 0005$  m.

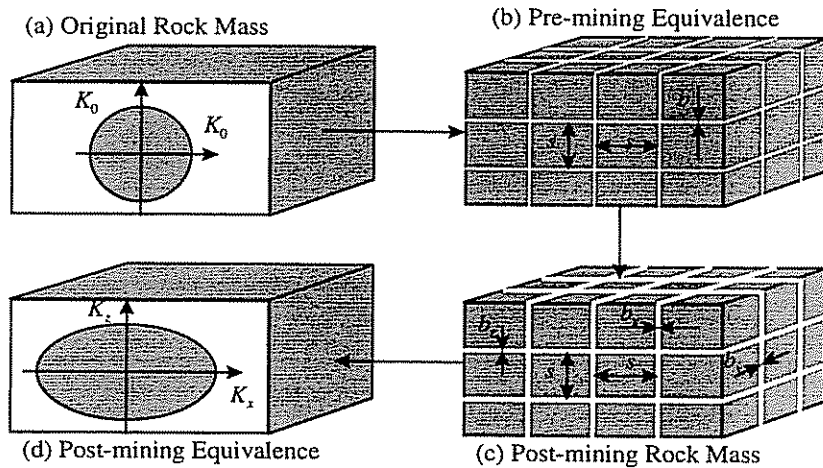


Fig. 3. Transformation processes of hydraulic conductivity models. The shaded circle in (a) represents that the conductivity field is isotropic. The shape in (d) represents that the conductivity field is anisotropic.

$$K_y = \frac{1}{2} K_{y0} [(1 + \beta_x \Delta \epsilon_x)^3 + (1 + \beta_z \Delta \epsilon_z)^3] \quad (8)$$

$$K_z = \frac{1}{2} K_{z0} [(1 + \beta_x \Delta \epsilon_x)^3 + (1 + \beta_y \Delta \epsilon_y)^3], \quad (9)$$

where

$$\beta_x = 1 + \frac{1 - R_m}{\frac{b_x}{s_x}} \quad (10)$$

$$\beta_y = 1 + \frac{1 - R_m}{\frac{b_y}{s_y}} \quad (11)$$

$$\beta_z = 1 + \frac{1 - R_m}{\frac{b_z}{s_z}} \quad (12)$$

and  $b_x/s_x$ ,  $b_y/s_y$  and  $b_z/s_z$  may be defined as a function of equivalent fracture porosity or fracture density.

Equations (7)–(9) may be rewritten as

$$R_x = \frac{K_x}{K_{x0}} = \frac{1}{2} [(1 + \beta_y \Delta \epsilon_y)^3 + (1 + \beta_z \Delta \epsilon_z)^3] \quad (13)$$

$$R_y = \frac{K_y}{K_{y0}} = \frac{1}{2} [(1 + \beta_x \Delta \epsilon_x)^3 + (1 + \beta_z \Delta \epsilon_z)^3] \quad (14)$$

$$R_z = \frac{K_z}{K_{z0}} = \frac{1}{2} [(1 + \beta_x \Delta \epsilon_x)^3 + (1 + \beta_y \Delta \epsilon_y)^3]. \quad (15)$$

For fractured media the post-mining hydraulic conductivities of the overburden are primarily controlled by mining-induced strains, original hydraulic conductivities, or the fracture parameters of spacing and aperture, as shown in equations (7)–(15). The mining-induced strains have been obtained through equation (3). The other parameters are discussed in the following.

### 3.2. Effects of $R_m$ on conductivity ratio

The post-mining hydraulic conductivity field can be uniquely defined by both the induced factor (the

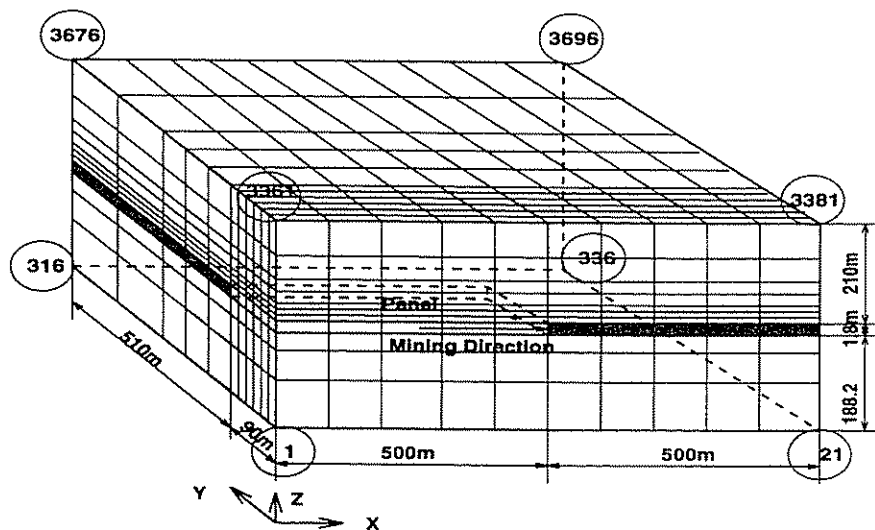


Fig. 4. FE models for both the determination of overburdened deformation and the post-mining hydrologic regime. Circled numbers are nodal numbers. Model used quarter symmetry of the panel, centered on the origin. Panel depth is 210 m below surface. Solid black represents un-mined coal.

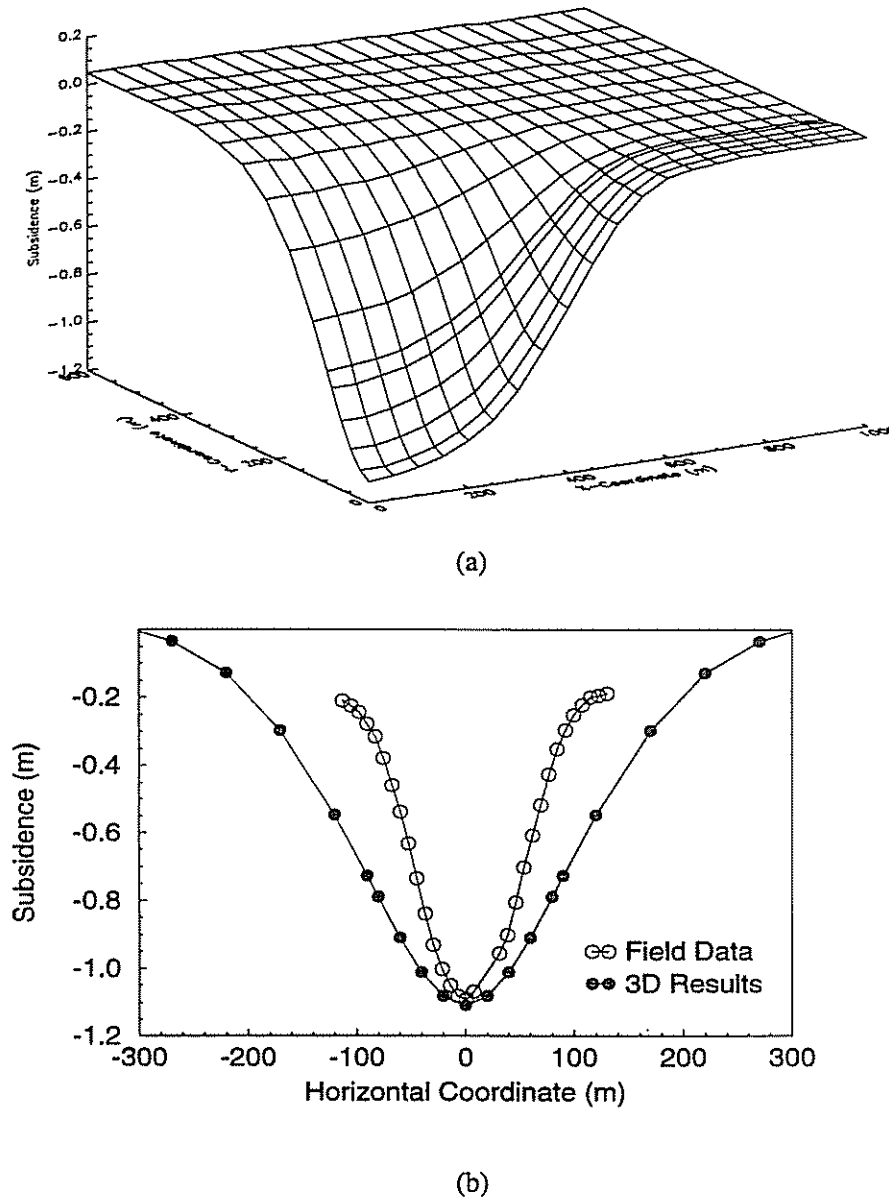


Fig. 5. Subsidence due to longwall mining: (a) subsidence cone, (b) comparison of model data with field data in the cross section of  $X = 0$ .

mining-induced strain field) and the intrinsic factors (the modulus reduction ratio,  $R_m$ , pre-mining hydraulic conductivity,  $K_0$ , or equivalent fracture spacing  $s$  and aperture  $b$ ).  $R_m$  is defined as the ratio of the elastic modulus of the rock mass to that of the intact rock. Actually, it is a measure of scale effect which is defined as the variation of test results with specimen sizes. This is apparent in that for application to field problems of subsidence, the laboratory values of deformation and rigidity moduli should be reduced at least an order to magnitude for both isotropic [17] and transversely isotropic [18]. The effects of  $R_m$  on changes in hydraulic conductivity are demonstrated in the following example.

Assuming  $\Delta\epsilon_z = 0$ ,  $b = 0.0005$  m, and  $s = 0.5$  m, the effects of  $R_m$ , as shown in equation (13) or (14), are illustrated in Fig. 2. The hydraulic conductivity may increase by up to 5 orders of magnitude when  $R_m$  changes from 0.0 to 1.0, as shown in Fig. 2. When the

modulus reduction ratio,  $R_m = 1$ , the rock mass and intact rock material moduli are identical and the strain is uniformly distributed between fractures and matrix. This results in the smallest possible change in conductivity. When  $R_m = 0$ , the strain is applied entirely to the fracture system and precipitates the largest possible change in conductivity. These values bound the possible ranges in behavior of the system in a natural, and mechanistically defensible manner.

The magnitude of  $R_m$  may be estimated by several methods. The scale effect of elastic modulus on three types of rock has been statistically studied [19] and the following relations were obtained by evaluating 35,600 test results in simple compression tests as  $R_m = 1/(1 + \alpha I)$ , where  $\alpha = 0.0859$  for limestone,  $\alpha = 0.1512$  for gneiss and  $\alpha = 0.0417$  for granite, with  $I$  representing fracture frequency. These relations may be used to estimate the magnitudes of  $R_m$ , directly.

The basic equation for the elastic deformation of a two-component medium in the direction perpendicular to the fracture is defined as [20]

$$\frac{b + s}{E_m} = \frac{s d\sigma}{E_r} + \frac{b d\sigma}{\xi E_r} \quad (16)$$

where  $d\sigma$  is the normal stress acting perpendicular to the fracture,  $\xi$  is the mineral contact area on the fracture wall,  $E_r$  is elastic modulus of the rock mass, and  $E_m$  is

elastic modulus of the rock matrix. For a rock mass containing fractures forming different angles with respect to the horizontal plane, the modulus reduction ratio,  $R_m$ , is obtained [20] as

$$R_m = \frac{E_m}{E_r} = \frac{1}{1 + \sum_{i=1}^N \eta_i (1 - \sin^4 \beta_i)} \quad (17)$$

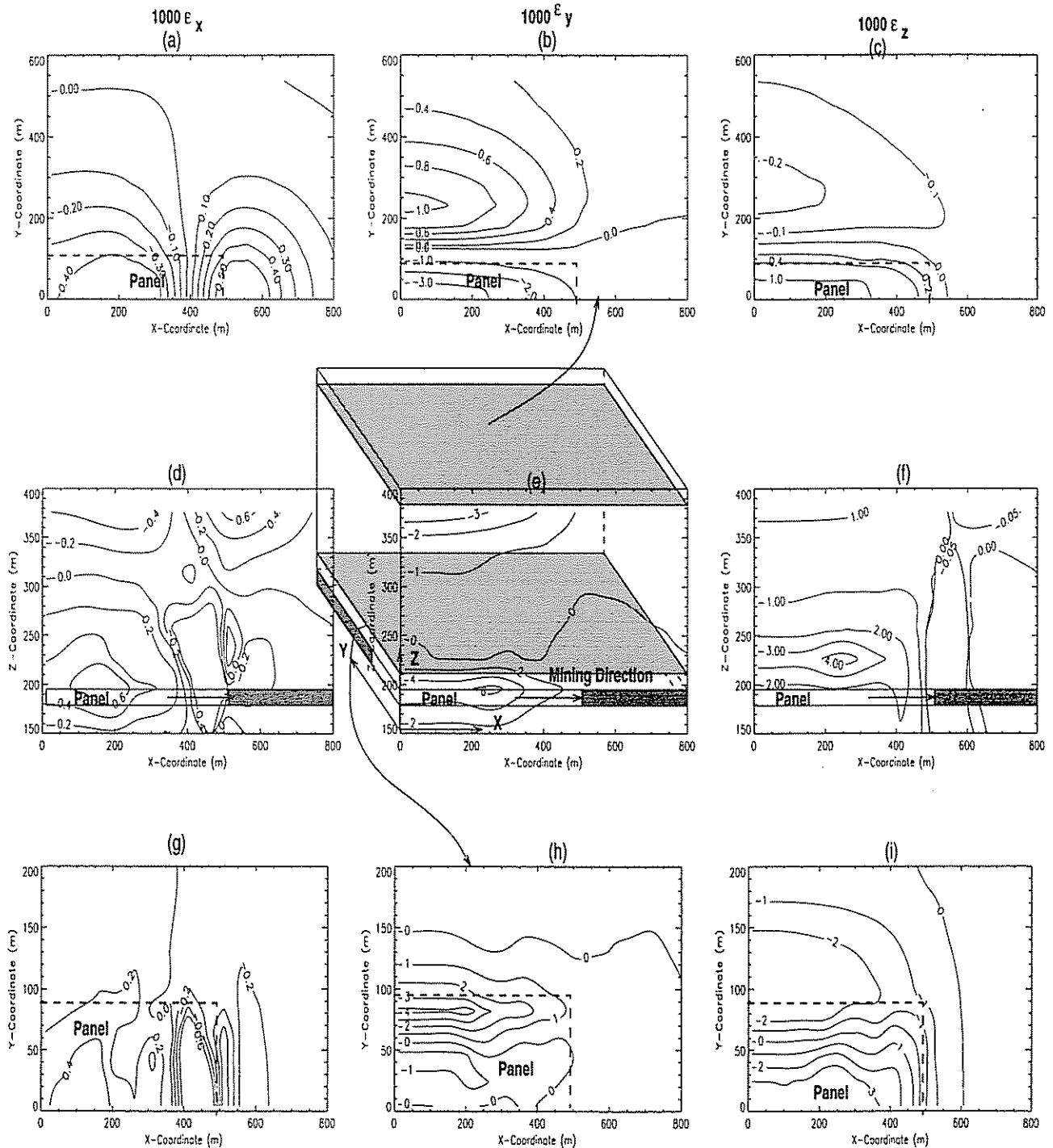


Fig. 6. Contours of normalized strains at different cross sections: (a), (b) and (c) represent strains in a horizontal plane in the near surface zone; (d), (e) and (f) represent strains in a vertical section along the panel centerline; (g), (h) and (i) represent strains in a horizontal plane immediately above the panel roof. Figures in the columns represent normal strains in the global  $x$ -,  $y$ - and  $z$ -directions, respectively.

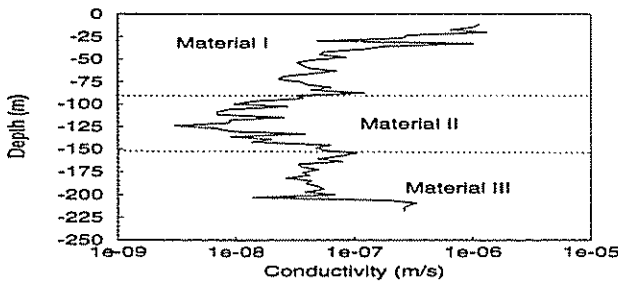


Fig. 7. Distribution of pre-mining hydraulic conductivities.

and

$$\eta_i = \frac{b}{s\xi_i} \tag{18}$$

where  $i$  is an index of fracture sets,  $\beta_i$  is the angle between the fracture and the area perpendicular to the direction of the desired modulus,  $\xi_i$  is geometric characteristic of the  $i$ th fracture set, and  $N$  is the number of the fracture sets in the rock mass. It is suggested [20] that  $\xi_i = 3 \times 10^{-4}$  be applied as a constant. Assuming three sets of orthogonal fractures coincident with the  $x$ -,  $y$ -, and  $z$ -directions, respectively, then  $N$  is equal to 3. Furthermore, assuming  $\eta_1 = \eta_2 = \eta_3 = b/s\xi$  and  $\xi = 3 \times 10^{-4}$ , then equation (17) becomes

$$R_m = \frac{1}{1 + \frac{10^4 b}{3s}} \tag{19}$$

As an alternative to the use of measured or estimated rock mass moduli, equation (19) may be used to determine the magnitude of  $R_m$ , directly.

### 3.3. Determination of post-mining hydraulic conductivity field

The process of determining the post-mining hydraulic conductivity is illustrated in Fig. 3. The *in situ* hydraulic conductivity is usually assumed to be isotropic, as shown in Fig. 3(a), because of the huge engineering scale (typically 200–350 m wide and up to 3000 m in length for a single panel). This isotropic continuous model is substituted by a discontinuous model, as shown in Fig. 3(b), with three identical sets of orthogonal fractures. The fracture aperture is obtained as

$$b = \left[ \frac{6\mu_k s K_0}{g} \right]^{1/3} \tag{20}$$

where  $s$  is the pre-mining fracture spacing, and  $\mu_k$  is kinematic viscosity of the fluid. The discontinuous model

is subjected to changes due to mechanical deformation such as longwall mining, as shown in Fig. 3(c) and the modified discontinuous model is then substituted by an equivalent porous anisotropic model, as shown in Fig. 3(d). Changes in the fracture aperture,  $\Delta b_x$ ,  $\Delta b_y$ , and  $\Delta b_z$ , are determined by mining-induced strains and fracture parameters. The mining-induced strains are obtained through equation (3), the fracture aperture is calculated by equation (20), and the modulus reduction ratio,  $R_m$ , may be obtained from equation (19), or equivalent. With the post-mining hydraulic conductivity field determined, the post-mining ground water flow regime can be evaluated.

### 4. EVALUATION OF POST-MINING GROUNDWATER FLOW

The resulting finite element formulation for the post-mining groundwater flow is symbolically defined as

$$\mathbf{K}_r \mathbf{h} = \mathbf{q} \tag{21}$$

where  $\mathbf{K}_r$  is the stiffness matrix of the fluid phase,  $\mathbf{h}$  is the nodal head vector, and  $\mathbf{q}$  is the nodal flux vector. The stiffness matrix for the fluid phase,  $\mathbf{K}_r$ , is defined as

$$\mathbf{K}_r = \iint_V \mathbf{T}^T \mathbf{K}(\Delta\epsilon) \mathbf{T} \, dx \, dy \, dz \tag{22}$$

where the property matrix  $\mathbf{K}(\Delta\epsilon)$  is analogous to the stress-strain matrix  $\mathbf{D}$  in solid elements and defined as (assuming the axes of the permeability tensor coincide with  $x$ ,  $y$  and  $z$ )

$$\mathbf{K}(\Delta\epsilon) = \begin{bmatrix} K_x & 0 & 0 \\ 0 & K_y & 0 \\ 0 & 0 & K_z \end{bmatrix} \tag{23}$$

and the  $\mathbf{T}$  matrix represents the derivatives of shape functions defined over individual elements, in the usual manner. Post-mining hydraulic conductivities,  $K_x$ ,  $K_y$  and  $K_z$ , are a function of mining-induced strains and determined through equations (7)–(9). For a free surface problem, the matrix  $\mathbf{K}_r$  is a function of total head  $h$ . A free surface is defined by two conditions [21] (1) fluid pressure  $p$  is equal to zero when atmospheric pressure is taken as the reference as

$$\frac{p}{\gamma_w} = h - z = 0 \tag{24}$$

where  $z$  is elevation head and  $\gamma_w$  is the unit weight of water; and (2) except in conditions of recharge

Table 1. Input parameters for the determination of mining impacts on ground water for case study 2

Material	$K_0$ (m/sec) determined based on Hasenfus <i>et al.</i> , 1990 [16]	$s$ (m) estimated	$b = \left( \frac{6\mu_k K_0}{g} \right)^{1/3}$ ( $\mu\text{m}$ )	$R_m = \left( 1 + \frac{10^4 b}{3s} \right)^{-1}$
I	$4.72 \times 10^{-7}$	0.5	66	0.69
II	$4.72 \times 10^{-9}$	0.3	12	0.88
III	$4.72 \times 10^{-6}$	0.5	142	0.50

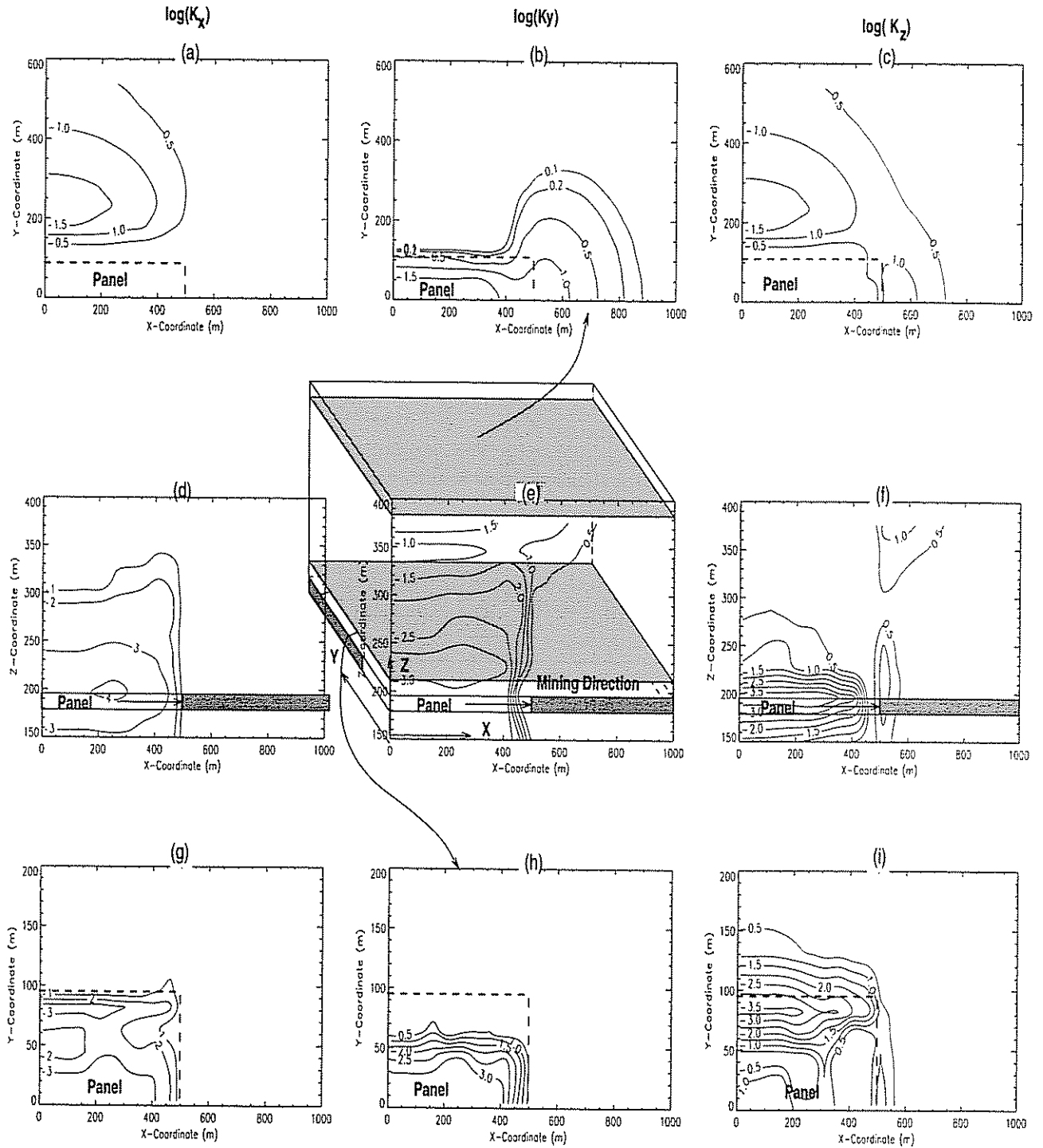


Fig. 8. Contours of ratios of post-mining hydraulic conductivities to pre-mining hydraulic conductivities at different cross sections: (a), (b) and (c) represent hydraulic conductivities in a horizontal plane in the near surface zone; (d), (e) and (f) represent hydraulic conductivities in a vertical section along the panel centerline; (g), (h) and (i) represent hydraulic conductivities in a horizontal plane immediately above the panel roof. Figures in the columns represent hydraulic conductivities in the global *x*-, *y*- and *z*-directions, respectively.

or evaporation, the flux across the free surface is zero as

$$\frac{\partial h}{\partial n} = q = 0 \tag{25}$$

where *q* is flux across the free surface, defined positive for evaporation. In the case of a free surface, the surface has to be determined as a part of the solution of the flow problem. The transient changes affecting this free surface

alter the geometry of the flow system so that the relationship between the changes at boundaries and the changes in piezometric heads and flows must be non-linear. As the mining-induced strain field typically changes the distribution of hydraulic conductivity magnitudes in all adjacent elements, traditional methods of representing the free surface by remeshing are cumbersome and not appropriate. Alternatively, a non-linear conductivity model is used to represent

changes in saturation in the overburden strata and enable representation of the ground water free surface [22,23]. The method requires a slightly more elaborate (non-linear) code than those remeshing methods used in practice today, however, for the complex conductivity distributions that develop in these studies, the method performs adequately. This kind of FE model has been developed in this study enabling the characteristics of the unsaturated zone above the free surface to develop in a physically natural manner.

Notice that matrix  $T$  remains fixed during solution procedure and  $K(\Delta\epsilon)$  has to be adapted at each iteration to represent the impact of desaturation. This is achieved at the end of each iteration by calculating the total head,  $h$ , for each element as

$$K(\Delta\epsilon) = \begin{cases} 1.0K(\Delta\epsilon) & h > z \\ 10^{-n}K(\Delta\epsilon) & h \leq z \end{cases} \quad (26)$$

where  $h$  is total head and  $z$  is elevation head, and  $n$  may be assigned any reasonable large numbers. The development of post-mining overburden desaturation zones is realized through modifying the conductivity magnitude to represent changes in saturation of the overburden strata.

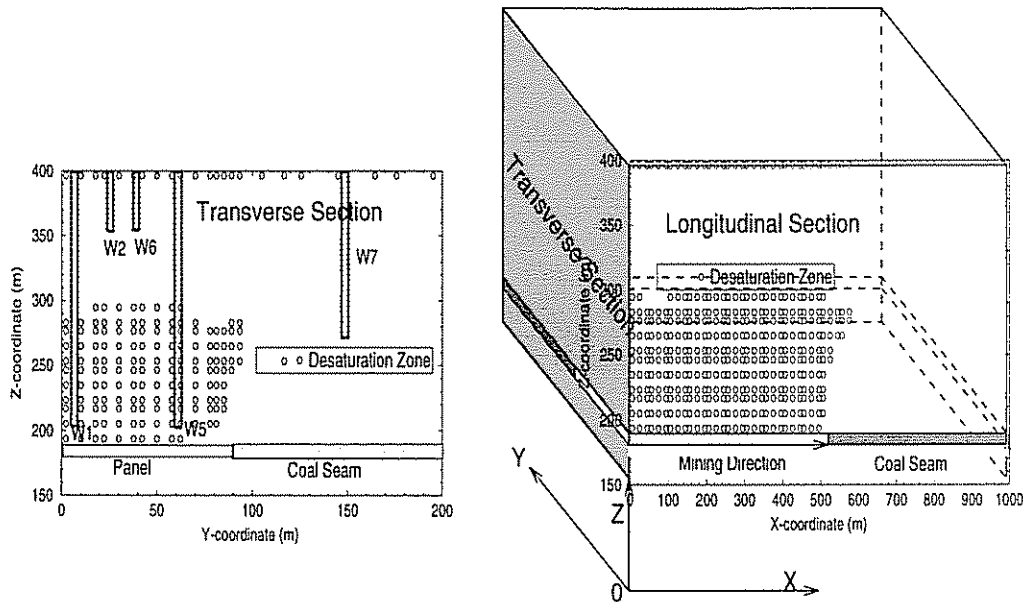
5. RESULTANT FE FORMULATION AND SOLUTION PROCEDURE

As a summary, the resultant finite element representation for the evaluation of the hydraulic conductivity enhancement and desaturation around mined panels is formulated as

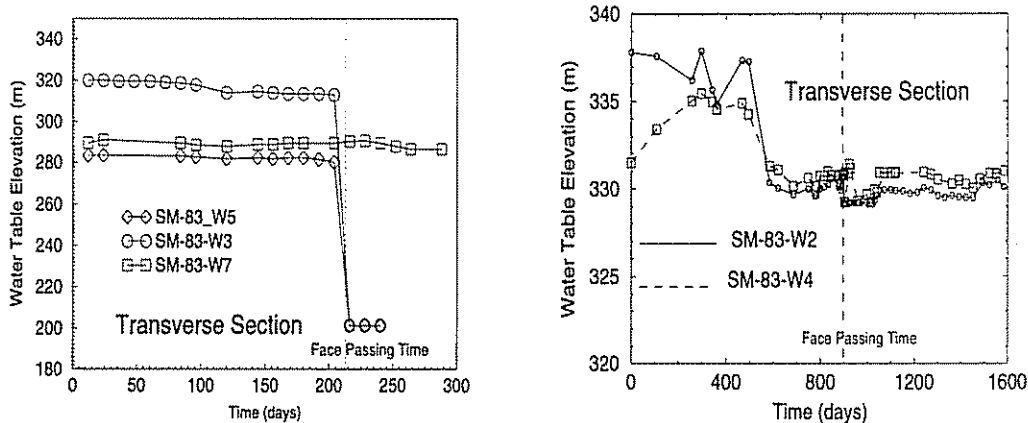
$$K_s(d)d = f \quad (27)$$

$$\Delta\epsilon = Bd \quad (28)$$

$$K_r h = q. \quad (29)$$



(a) Distribution of post-mining overburden desaturation



(b) Observed water level fluctuation in monitoring wells

Fig. 9. Distribution of post-mining overburden desaturation zones and the observed water level fluctuation in monitoring wells: (a) well locations are shown with completion intervals defined, relative to the geometry of the transverse section. Predictions of desaturation zones are identified by small circles, (b) observed water well records during undermining relative to time of face passage.

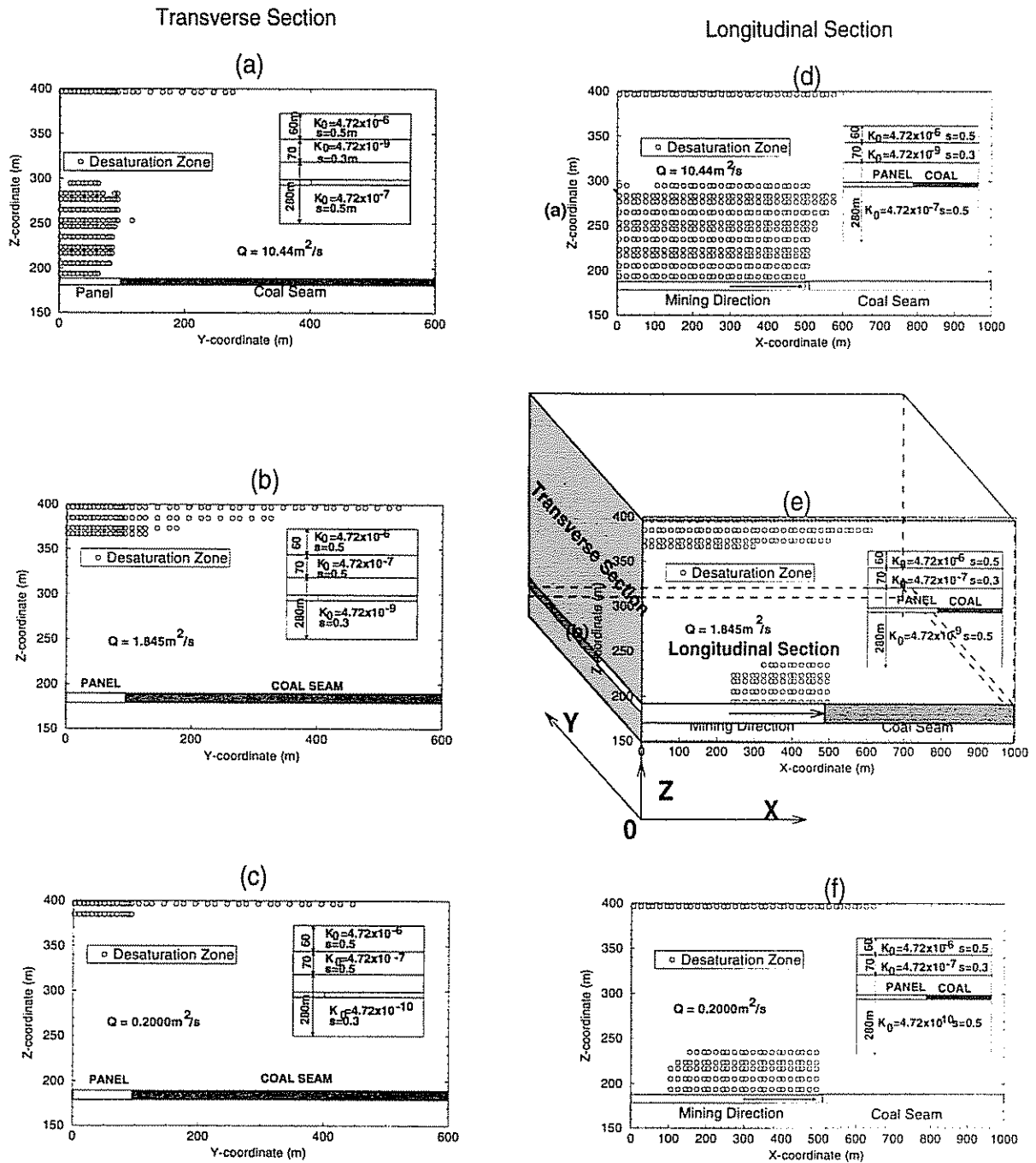


Fig. 10. Distribution of overburdened desaturation zones under different pre-mining hydraulic conductivity fields. Units for  $K_0$  and  $s$  are m/sec and m, respectively.

Equations (27)–(29) are coupled through the relations between the mining-induced strains and the post-mining hydraulic conductivities, as defined in the following

$$K_x = \frac{1}{2} K_{x,0} [(1 + \beta_y \Delta \epsilon_y)^3 + (1 + \beta_z \Delta \epsilon_z)^3] \quad (30)$$

$$K_y = \frac{1}{2} K_{y,0} [(1 + \beta_x \Delta \epsilon_x)^3 + (1 + \beta_z \Delta \epsilon_z)^3] \quad (31)$$

$$K_z = \frac{1}{2} K_{z,0} [(1 + \beta_x \Delta \epsilon_x)^3 + (1 + \beta_y \Delta \epsilon_y)^3] \quad (32)$$

The hydraulic conductivity enhancement and desaturation around mined panels are evaluated through the

following straightforward steps: 1. The strain field that develops around a longwall panel as a result of mining is obtained through solving equations (27) and (28), using a non-linear FE model that accommodates the influence of material failure and self-weight; 2. From this predicted strain field, and from knowledge of the pre-mining hydraulic properties of the overlying strata, post-mining hydraulic conductivity field is obtained through solving equations (30)–(32); 3. With the post-mining hydraulic conductivity field determined, the post-mining hydrologic system is subsequently defined through solving equation (29), using a ground water model. Again, determination of the post-mining hydrologic system utilizes a non-linear FE model that

incorporates the development of the ground water free surface. The validation of the resultant FE model is well documented in studies [8,14,24–26]. The FE model is also applied to a well instrumented longwall mine site as a two-dimensional example [26]. The following documents the application of this FE model to another well instrumented longwall mine site as a three-dimensional example. Through this application, the complex three-dimensional hydraulic response of overburden to longwall mining around the advancing mining face are thoroughly examined. These results are reported in the following sections.

## 6. APPLICATION OF THE FEM MODEL

An extensive hydrological and geomechanical monitoring program was conducted at a longwall coal mine in West Virginia [16]. Ground water levels, pre-mining hydraulic conductivity, overburden movement, and surface subsidence relative to the passage of the longwall panel were obtained through this monitoring program. Based on this information, the mining-induced overburden strain field, the post-mining overburden hydraulic conductivity field and the post-mining ground water flow regime are evaluated. Results of the evaluation are verified against the *in situ* monitoring results.

### 6.1. Site specification and field monitoring

The mine is located within the Pittsburgh seam, with an average extraction thickness at the study site ranging from 1.7 to 1.8 m (5.5 to 6 feet). The instrumented panel is 183 m (600 feet) wide by 2195 m (7200 feet) long. The overburden monitoring test site is located at approximately center-panel length. The test site lies on top of a broad crest at the end of a long steep-side ridge. Relief to the stream valley below is 91–122 m (300–400 feet). The coal seam is approximately 213–219 m (700–720 feet) deep at the test site. The mined seam lies directly beneath about 85 m (280 feet) of highly competent limestone and sandstone strata as contrasted with the low strength shales and claystones close to the surface.

The shallow water-bearing strata at the test location are considered to be perched or semiperched aquifers, which consist of a vertical succession of water tables separated by unsaturated zones. Low permeability shales and claystones impede the downward migration of ground water, and water levels decrease as well depth increases. Aquifer recharge is almost entirely from precipitation in the form of snow and rain, and discharge occurs via springs, seeps along hillsides and via evapotranspiration. Pre-mining water levels in wells drilled within the upper 60 m (200 feet) fluctuated widely with seasonal changes in precipitation patterns and evapotranspiration. Steep topography is known to have played an important role in shallow aquifer water level fluctuation, since the high runoff and small recharge area greatly limit recharge. Pre-mining water levels below 122 m (400 feet) remained fairly constant.

Ground water monitoring was conducted in a total of eight monitoring wells and one private well. Six of the

monitoring wells and the private well were located near the panel-center. Three of those wells (W1, W3 and W5) were completed to a depth of 183 m (600 feet). Of the two wells drilled over the panel headgate, well W7 was completed to a depth of 123 m (405 feet). The other four wells W2, W4, W6 and the private well were completed to a depth of less than 62 m (200 feet).

### 6.2. Field ground water monitoring results

Hydraulic responses were observed through eight monitoring wells. In general, water levels in shallow wells [W2, W4 and W6, less than 62 m (200 feet) deep] and near center-panel were lowered (or went dry) within 1 month of being undermined, then recovered to near pre-mining levels, 4–5 months after mining. Sustained post-mining water levels in these shallow wells exhibited less fluctuation and were slightly lower than average pre-mining levels. The 183-m (600-foot) deep wells (W1, W3, and W5) went dry after the face had passed 15 m (50 feet) and did not recover. The 123-m (405-foot) well (W7) over the headgate was relatively unaffected in the long term by passage of the face.

### 6.3. Three-dimensional numerical model

The three-dimensional FE model developed for both the determination of overburden deformation and post-mining hydrologic effects is illustrated in Fig. 4. Boundary mesh deformations in the  $x$ -direction at the cross sections of  $X = 0$  and  $X = 1000$  m, in the  $y$ -direction at the cross sections of  $Y = 0$  and  $Y = 600$  m, and in the  $z$ -direction at the bottom ( $Z = 0$ ) are constrained for the determination of overburden deformation. No flow boundary conditions are applied at the cross sections of  $X = 0$  and  $Y = 0$ , and constant head boundary conditions are applied ( $h = 400$  m) at the cross sections of  $X = 1000$  m and  $Y = 600$  m and around the panel ( $h = 188.2$  m for the floor,  $h = 190$  m for the roof). This enables the post-mining ground water regime to be determined, with the inclusion of deformational effects.

The values of the modulus of elasticity for the overburden are assumed as  $E = 4 \times 10^9$  Pa and 0.30, respectively. The post-failure values of the Poisson ratio and elastic modulus in extensional elements, are obtained as 0.45 and  $E/4$ , respectively, by matching the maximum model subsidence with the field measured magnitude.

### 6.4. Distribution of mining-induced strains

The model subsidence cone is illustrated in Fig. 5(a) and the final subsidence profile at the cross section of  $X = 0$  is compared with field data in Fig. 5(b). It is apparent that the model subsidence profile is flatter than the field measured one. This may be due to the possible discontinuous deformation of overburden which is not incorporated in the continuous deformation model. Nevertheless, the mismatch between the measured and modeled subsidence profiles may be considered adequate for the subsequent analyses.

The strain field, modulated by the surface subsidence profile, is illustrated in Fig. 6. Apparent from these figures is that significant mining-induced overburden extensional deformation is restricted to shallow depths (less than 100 m deep) ahead of the advancing face, but more significant mining-induced extensional deformation develops behind the advancing face, particularly in the caving zone and in shear zones above the abutments.

### 6.5. Evaluation of post-mining conductivity field

Post-mining hydraulic conductivities for the study [16] are defined as a function of mining-induced strain field and the pre-mining hydraulic conductivity field (or fracture parameters). The mining-induced strain magnitudes, defined by evaluation of the subsidence profile, are incorporated directly into the analysis. This strain field, together with the pre-mining hydraulic conductivity, is used to determine the post-mining hydraulic conductivity field. Pre-mining hydraulic conductivity magnitudes for the overburden are determined according to the pre-mining conductivity measurements, as shown in Fig. 7 [16]. The overburden may be divided into three material units to approximately represent the real distribution of conductivity, comprising a central aquitard, bounded above and below by more conductive units. The thicknesses for each material unit are 60, 70, and 60 m, respectively. The pre-mining hydraulic conductivity field is assumed to be isotropic and is substituted by a discontinuous flow model with three identical sets of orthogonal fractures. The fracture parameters of spacing, aperture and modulus reduction ratio are determined from the pre-mining hydraulic conductivity with estimated magnitudes of fracture spacing. Input parameters for the determination of mining impacts on the ground water resource are listed in Table 1.

The ratios of post-mining hydraulic conductivities to pre-mining hydraulic conductivities at different cross sections are illustrated in Fig. 8. The figure illustrates that significant conductivity increases are restricted to shallow depths (less than 100 m deep) ahead of the advancing face, but more significant conductivity increases develop behind the advancing face, particularly in the caving zone, and in shear zones above the abutments.

### 6.6. Three-dimensional effects

As the working face advances, the abutment at the face experiences a truly three-dimensional stress regime that includes the stress-concentration effects at the panel corner. If damage and strains are non-linear and irrecoverable, this may leave remnant changes in hydraulic conductivities that are larger than the magnitudes predicted by the plane-strain FE model. The importance of this effect is observed, as shown in Fig. 8(b), (c) and (f). As shown in Fig. 8(b), the region of transverse hydraulic conductivity enhancement significantly shrinks behind the working face. This suggests that the increase of hydraulic conductivity in the

transverse direction will be underestimated by the plane-strain FE model. As shown in Fig. 8(c) and (f), significant increase of hydraulic conductivity in the vertical direction may occur ahead of the working face. The remnant increase may counteract the decrease in the vertical hydraulic conductivity predicted by the plane-strain FE model [26].

### 6.7. Determination of overburden desaturation

The impacts of longwall mining on ground water resources are evaluated in terms of the distribution of overburden desaturation zones as defined in the long-term, where steady-state flow conditions prevail. This represents behavior following passage of the longwall face, and defines the most important behavior from a practical standpoint. The evaluation of desaturation zone extents is important in defining expected survivability of water supply wells to undermining.

The distribution of post-mining overburden desaturation zones, evaluated based on the post-mining hydraulic conductivity field and the applied boundary conditions, with the observed water level fluctuation in monitoring wells, are illustrated in Fig. 9. Under the applied boundary conditions for the flow model, two separate desaturation zones are developed following mining of the panel. One is at the surface (about 10 m in depth), and the other is directly above the panel (about 175 m in depth), as illustrated in Figure 9(a). The wells completed within the range of 10–120 m in depth (W2, W4, W6, W7, and the private well) will likely survive mining because they are located within the post-mining saturated zone (aquifer) and wells completed within the range of 120–210 m in depth (W1, W3, and W5) may drain because they are located directly within the post-mining desaturation zone. These model results are consistent with both observed results, as reported in Fig. 9(b). The observed results indicate that the impacts of longwall mining on shallow wells are extremely localized with respect to the mining front. However, the impacts of longwall mining on deep wells may be extensive, permanent and unlikely to recover.

### 6.8. Effects of less permeable layers

Assuming that the pre-mining hydraulic conductivity of less permeable layers present above the panel is isotropic, behavior may be represented by an equivalent porous medium. This may be defined, according to equation (17), where the modulus reduction ratio,  $R_m$ , can be defined as

$$R_m = \frac{1}{1 + \frac{10^4}{3} \left( \frac{6\mu K_0}{gs^2} \right)^{1/3}} \quad (33)$$

If there are no fractures ( $s \rightarrow \infty$ ), equation (33) becomes  $R_m = 1.0$ . According to equations (13)–(15) conductivity ratios ( $R_x$ ,  $R_y$ , and  $R_z$ ) can be defined as

$$R_x = \frac{1}{2} [1 + \Delta\epsilon_x]^3 + (1 + \Delta\epsilon_z)^3 \quad (34)$$

$$R_x = \frac{1}{2} [1 + \Delta\epsilon_x]^3 + (1 + \Delta\epsilon_x)^3 \quad (35)$$

$$R_z = \frac{1}{2} [1 + \Delta\epsilon_z]^3 + (1 + \Delta\epsilon_z)^3 \quad (36)$$

Physically, equations (34)–(36) define that the strain is uniformly distributed between fractures and matrix. This results in the smallest possible change in hydraulic conductivity due to longwall mining.

Three different combinations for the distribution of the pre-mining hydraulic conductivity are chosen for the numerical model as illustrated in Fig. 4. This representation is used to investigate the effects of less permeable layers on the hydraulic impacts of longwall mining. The hydraulic parameters used in the model, and the numerical results are shown in Fig. 10. The effects of less permeable layers are evaluated in terms of the distribution of post-mining overburden desaturation zones and drainage into the mine. It is apparent that the distribution of post-mining overburden desaturation zones and drainage into the mine are determined by both the location of the less permeable layer and the magnitude of its pre-mining hydraulic conductivity. The potential for dewatering the shallow aquifer may be reduced by the presence of a less permeable layer. If two aquifers are separated by this layer, however, the deep aquifer may be severely dewatered as shown in Fig. 10(a) and (d). The magnitude of the pre-mining hydraulic conductivity of a less permeable layer may affect both the distribution of post-mining overburden desaturation zones and the drainage into the mine if the aquifer is separated from the mine by this less permeable layer, as shown in Fig. 10(b), (c), (e) and (f).

## 7. CONCLUSIONS

Three-dimensional effects of hydraulic conductivity enhancement and overburden desaturation around a longwall mining advancing face are evaluated through use of a three-dimensional coupled finite element hydromechanical model.

The complex hydromechanical coupling process between mining-induced overburden deformation and desaturation is represented through three-dimensional relations between induced strain and change in hydraulic conductivity developed in this study. Data requirements for the model are minimal because the displacement boundary condition is successfully applied to represent the process of coal extraction.

The complex distribution of post-mining hydraulic conductivities around the advancing face is determined by the mining layout, particularly the mining geometry such as mining depth, panel width and height, with extent largely modulated by the presence and the location of flatlying layers of low conductivity. Apparent from this study is that significant hydraulic conductivity increases are restricted to the shallow depths ahead of the advancing face, but more significant increases develop behind the advancing face, particularly in the caving zone, and in the shear zones above the abutments.

Because significant hydraulic conductivity increases behind the advancing face are much larger than those ahead of it, both in the surface zone and in the immediate zones along the panel edges, longitudinal drainage may play a very important role in evaluating the impact of longwall mining on ground water levels around the mining front. Dramatic changes in hydraulic conductivity around the advancing face may also cause dramatic changes in ground water levels. However, these changes may be modulated by the presence of flatlying less permeable layers. If the presence of a flatlying less permeable layer cannot prevent the direct connection between the surface zone and the immediate zone of hydraulic conductivity enhancement, water level fluctuations within both zones result following undermining. If the presence of a flatlying less permeable layer can prevent the direct connection between the surface zone and the immediate zone of hydraulic conductivity enhancement, water levels within the surface zone will fluctuate much less significant than those within the immediate zone. These conclusions are consistent with observed results.

Although this model is applied to a particular longwall mine site, conclusions drawn from this study may be used to explain observed results from other mining situations. However, cautions about the FE model limitations should be made when applying these conclusions. These limitations include that the FE model for the solid phase does not incorporate the potential discontinuous deformation of the overburden and that the relations between mining-induced strains and post-mining hydraulic conductivities do not include the effect of shear strains. These limitations need to be addressed in the future work.

*Acknowledgements*—This work has been partially supported by the National Science Foundation, U.S.A., under Grant No. CMS-9209059, and by the National Mined Land Reclamation Center under Grant No. CO388962. This support is gratefully acknowledged. The authors also thank two anonymous reviewers and the Editor for providing critical comments and constructive suggestions in revising the manuscript.

*Accepted for publication 12 June 1997.*

## REFERENCES

1. Neate, C. J. and Whittaker, B. J., Influence of proximity of longwall mining on strata permeability and ground water. *Proceedings of U.S. 22nd Symposium on Rock Mechanics*, pp. 217–224, The University of Texas at Austin (1979).
2. Booth, C. J., Hydrogeologic impacts of underground (longwall) mining in the Illinois basin. In *Proceedings of Third Workshop on Surface Subsidence due to Underground Mining* (Edited by Peng S.), pp. 222–227, Department on Mining Engineering, West Virginia University, Morgantown (1992).
3. Walker, J. S., Case study of the effects of longwall mining induced subsidence on shallow ground water sources in the Northern Appalachian Coalfield. R19198, Bureau of Mines, United States Department of the Interior (1988).
4. Van Roosendaal, D. J., *et al.*, Overburden deformation and hydrological changes due to longwall mine subsidence in Illinois. In *Proceedings of 3rd Conference on Ground Control Problems in the Illinois Coal Basin* (Edited by Chugh Y. P.), pp. 73–82, Mt Vernon, IL (1990).

5. Mateic, R. J., Trevits, M. A. and Swinehart, T., A case study of longwall mining and near-surface hydrological response. *Proceedings of American Mining Congress-Coal Convention*, Pittsburgh, PA (1991).
6. Matetic, R. J. and Trevits, M., Longwall mining and its effects on ground water quantity and quality at a mine site in the northern Appalachian coal field. *Proceedings of FOCUS Conference on Eastern Regional Ground Water Issues*, 13-15 October, Newton, MA, USA (1992).
7. Matetic, R. J., An assessment of longwall mining-induced changes in the ground water system. *Proceedings of FOCUS Conference on Eastern Regional Water Issues*, 27-29 September, Dublin, OH, USA (1993).
8. Matetic, R. J., Liu, J. and Elsworth, D., Modeling the effects of longwall mining on the ground water system. In *Proceedings of the 35th U.S. Symposium on Rock Mechanics* (Edited by Daemen J. J. K. and Schiltz R. A.), pp. 639-644, University of Nevada, Reno, USA (1995).
9. Bai, M. and Elsworth, D., Transient poroelastic response of equivalent porous media over a mining panel. *Engng Geol.* 35, 49-64 (1993).
10. Bai, M. and Elsworth, D., Dual-porosity poroelastic approach to behavior of porous media over a mining panel. *Trans. Inst. Min. and Met.* 102, A114-A124 (1993).
11. Bai, M. and Elsworth, D., Modeling of subsidence and stress-dependent hydraulic conductivity for intact rock and fractured porous media. *Rock Mech. Rock Engng.* 27(4), 209-234 (1994).
12. Bai, M. and Elsworth, D., Influence of mining geometry on mine hydro-geo-mechanics. *Trans. Soc. Min. Engrs* 296, 1856-1863 (1995).
13. Ouyang, Z. and Elsworth, D., Evaluation of groundwater flow into mining panels. *Int. J. Rock Mech. Min. Sci. Geomech. Abstr.* 30(2), 71-79 (1993).
14. Liu, J., Topographic influences of longwall mining on water supplies. Master's thesis, Department of Mineral Engineering, The Pennsylvania State University (1994).
15. Elsworth, D., Liu, J. and Ouyang, Z., Some approaches determine the potential influence of longwall mining on ground water resources. *Proceedings of Int. Land Reclamation and Mine Drainage Conference and 3rd Int. Conference on the Abatement of Acidic Drainage*, Vol. IV, pp. 172-179, Pittsburgh, PA (1994).
16. Hasenfuls, G. J., Johnson, K. L. and Su, D. H. W., A hydromechanical study of overburden aquifer response to longwall mining. In *Proceedings of 7th Int. Conference on Ground Control in Mining* (Edited by Peng S. S.), pp. 149-162 (1990).
17. Voight, B. and Pariseau, W., State of predictive art in subsidence engineering. *J. Soil Mech. Foundations Division* (1970).
18. Berry, D. S., Ground movement considered as an elastic phenomenon. *The Mining Engr* 37, 28-39 (1963).
19. Peres-Rodrigues, F., About Inec experience on scale effects in the deformability of rocks. In *Scale Effects in Rock Masses*, pp. 155-164 (1990).
20. Chernyshev, S. N. and Dearman, W. R., *Rock Fractures*. Butterworth-Heinemann (1991).
21. Dassargues, A., Transient simulation of water table aquifers using a pressure dependent storage law. In *Computational Modeling of Free and Moving Boundary Problems II* (Edited by Wrobel L. C. and Brebbia C. A.), pp. 3-10. Computational Mechanics Publishers (1992).
22. Bathe, K. and Khoshgoftaar, M. R., Finite element free surface seepage analysis without mesh iteration. *Int. J. Numer. Methods Anal. Methods Geomech.* 3, 13-22 (1979).
23. Dysli, M. and Rybisar, J., Coupled models and free surface seepage analysis without mesh iteration. In *Numerical Methods in Geomechanics*, Vol. 2 (Edited by Swoboda G.), pp. 791-795. Balkema (1988).
24. Elsworth, D. and Liu, J., Topographic influence of longwall mining on ground water supplies. *Ground Water*, Autumn (1994).
25. Liu, J., Numerical studies toward a determination of the impact of longwall mining on ground water resources. Ph.D. thesis, The Pennsylvania State University, University Park, PA 16802 (1996).
26. Liu, J., Elsworth, D. and Matetic, R. J., Evaluation of post-mining ground water regime. *Hydrological Processes* (in press) (1997).